NASA TN D-997

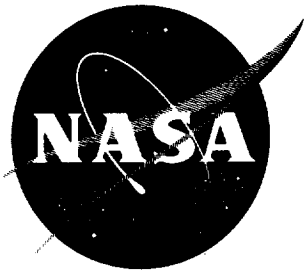

TECHNICAL NOTE

D-997

IN-FLIGHT NOISE MEASUREMENTS FOR THREE PROJECT MERCURY VEHICLES

By William H. Mayes, David A. Hilton,
and Charles A. Hardesty

Langley Research Center
Langley Air Force Base, Va.

NATIONAL AERONAUTICS AND SPACE ADMINISTRATION

WASHINGTON January 1962

NATIONAL AERONAUTICS AND SPACE ADMINISTRATION

TECHNICAL NOTE D-997

IN-FLIGHT NOISE MEASUREMENTS FOR THREE PROJECT MERCURY VEHICLES

By William H. Mayes, David A. Hilton,
and Charles A. Hardesty

SUMMARY

In-flight noise measurements have been made for three vehicles of the Project Mercury program. Inside noise measurements have been made for the three vehicles and measurements of external aerodynamic surface-pressure fluctuations have been made for one of the vehicles. The main sources of noise are the rocket engines during the launch phase and the noise of aerodynamic origin during the exit phase of the flight. The rocket noise was a maximum at lift-off and decreased rapidly as the vehicle gained altitude and speed. The noise of aerodynamic origin increased generally as the dynamic pressure increased and also was affected significantly by the Mach number and the external contouring of the vehicle.

INTRODUCTION

In connection with the Project Mercury program there has been serious concern for possible noise problems such as sonic fatigue of the spacecraft heat-shield shingles, equipment malfunction, interrupted voice communications, and Astronaut comfort and safety. Consequently, noise measuring equipment to obtain in-flight information relative to these problems was included in a series of development tests. Although the data obtained apply directly to the Mercury configuration, it is believed that they are also of interest for all types of ground-launched space vehicles.

Some analytical studies (refs. 1, 2, and 3) have been made for the purpose of predicting the levels and spectra of the inside noise environments of the ground-launched space vehicles; in particular, these studies have been concerned with the launch and reentry phases of the flight. The value of flight data for noise of aerodynamic origin is enhanced by the well-known difficulty of obtaining such data in the wind tunnel. Very little measured in-flight data have been reported to date, especially for large low-acceleration vehicles of a type suitable for manned

flight. Some preliminary results of internal and external noise measurements from Big Joe and Little Joe vehicles of the Mercury program as obtained from onboard recordings are presented in reference 4.

The main purpose of the present paper is to present detailed information relating to the in-flight noise measurements from three development vehicles of the Mercury program which were designed and constructed at the Langley Research Center and tested at the NASA Wallops Station. Data are presented for full-sized Mercury spacecraft configurations of simplified construction for which the escape tower mechanism was in place. Results are included for Mach numbers up to 5.7, for dynamic pressures up to about 3,000 lb/sq ft, for escape-system engine firings at various altitudes, and for launch-vehicle engines operative and inoperative.

SYMBOLS

h	altitude, ft
M	Mach number
$\sqrt{\overline{p^2}}$	inside noise pressure or external surface pressure, lb/sq ft
q	dynamic pressure, lb/sq ft
r	radius, in.
t	time from lift-off, sec

APPARATUS AND METHODS

Description and Operating Conditions of Test Vehicles

Photographs of the three test vehicles in their launching attitudes at the NASA Wallops Station launching area are shown in figure 1. Figure 1(a) shows a photograph of the Mercury spacecraft and the Little Joe 1B vehicle which were used primarily to test the escape system at conditions corresponding to the maximum dynamic pressure anticipated with the Mercury spacecraft. Figure 1(b) is a photograph of the Mercury spacecraft and the Little Joe 2 vehicle which were used primarily to check the escape system at extreme altitude conditions. Figure 1(c) is a photograph of a spacecraft designed to test the escape system at very low altitude conditions. The vehicles pictured in figures 1(a), 1(b), and 1(c) will hereafter be referred to as vehicles A, B, and C, respectively.

The dynamic pressures, altitudes, and Mach numbers for which noise data were obtained are shown as a function of time in figures 2, 3, and 4 for vehicles A, B, and C, respectively. Noted in figures 2 and 3 are the times of appropriate events such as pylon separation, escape rocket firing, and second-stage ignition.

The variations of ambient temperature and pressure obtained from rawinsonde observations are shown for the appropriate flights in figure 5 as functions of altitude; for comparison, the International Civil Aviation Organization (ICAO) standard atmospheric conditions (ref. 5) of temperature and pressure are also shown.

Vehicle A.- Vehicle A was launched at an angle of about 20° from the vertical and on a trajectory such that data were obtained for dynamic pressures up to about 2,200 lb/sq ft, for altitudes up to about 44,000 feet, and for Mach numbers up to about 2.1. The overall length of the vehicle, measured from the rearward extremity of the control fin to the forward portion of the escape motor housing, was about 49 feet. The distance from the launch-vehicle engine nozzles to the base of the instrumented spacecraft was approximately 21 feet. The total thrust of the solid-fuel launch-vehicle engines at lift-off was about 240,000 pounds.

Vehicle B.- Vehicle B was launched at an angle of about 12° from the vertical and on a trajectory such that data were obtained at dynamic pressures up to 3,000 lb/sq ft, altitudes up to 160,000 feet, and Mach numbers up to about 5.7. The total thrust of the solid-fuel launch-vehicle engines at lift-off was about 260,000 pounds. The external dimensions were roughly the same as those of vehicle A.

Vehicle C.- Vehicle C was launched on a trajectory having an angle of about 19° from the vertical. This vehicle was propelled only by the escape-system rockets which had a total thrust of approximately 60,000 pounds. Noise data were obtained for dynamic pressures up to about 400 lb/sq ft, altitudes up to about 450 feet, and Mach numbers up to about 0.5.

Description of the Spacecraft

A sketch of the instrumented spacecraft showing some of the details of its construction is shown in figure 6. Of particular significance are the heavy base plate, the conical walls of relatively light construction, the pressurized interior compartments of the spacecraft, and the 60,000-pound-thrust escape rocket motor having three exhaust nozzles spaced 120° apart. The thrust axes of the escape rocket nozzles were canted about 19° from the vehicle center line. The flight data were recorded with the aid of onboard missile tape

recorders which were recovered after the flights. All vehicles contained an internal microphone located at a position roughly equivalent to the proposed location of the Astronaut's head. For vehicle A only, a microphone was located in the unpressurized region of the spacecraft in order that the external surface pressures could be measured. (See insert sketch of fig. 6.)

The overall dimensions of the spacecraft and escape-system accessories were about 21 feet, as indicated in figure 6, and the escape rocket exhaust nozzles were about 16 feet from the base of the spacecraft. The dimensions and the component illustrations noted in the figure apply equally to all three vehicles since in these tests only minor differences existed in the spacecraft and the escape-tower configuration. One notable exception is the aerodynamic spoiler which was included only on the spacecraft of vehicle A. The details of the geometry of this spoiler are shown schematically in figure 6; the spoiler may also be seen at the top of the spacecraft in figure 1(a).

The conical sidewalls of the spacecraft of vehicles A and B were constructed of a 0.2-inch thickness of fiber glass and a 0.1-inch thickness of a charring ablation material, the resulting surface density being about 2.0 lb/sq ft. The conical sidewalls for the spacecraft of vehicle C were constructed of 1/8-inch steel plate with a resulting surface density of about 5 lb/sq ft.

Instrumentation

The instrumentation used for obtaining the noise measurements consisted of microphone systems and an onboard tape recorder, all of which were recovered by parachute techniques at the conclusion of the test. The main components of the noise-measuring instrumentation and their orientations in the test spacecraft are shown in figure 6. Care was taken to shock-mount the microphones; in order to minimize the possibility of spurious readings caused by acceleration of the vehicle, the microphones were mounted in such a way that the sensitive diaphragms were oriented in a plane parallel to the thrust axis of the vehicle.

The frequency responses of the condenser microphones used for the internal noise measurements were flat within ±2 decibels from 10 cps to 10,000 cps. The frequency response of the commercially available probe microphone system used for the external surface-pressure measurements was flat within ±2 decibels from 10 cps to 5,000 cps. For vehicles A and B the missile tape recorder was operated in an FM record mode and the overall frequency response of the system was from 10 cps to about 7,900 cps with a dynamic range of approximately 35 decibels. For vehicle C the same type of tape recorder was operated in a direct record mode, the system response was within ±3 decibels for the

frequency range of 100 cps to 10,000 cps, and the dynamic range was about 50 decibels. The total available recording time for each test was approximately 4 minutes.

The tape records were played back through a compensating unit to correct possible tape speed variations during flight. Frequency analyses were then obtained for the data of vehicles A and B with the use of a one-third octave band analyzer and graphic level recorder. The data from vehicle C were analyzed with a 100-cps constant bandwidth analyzer, and these data were adjusted to one-third octave bandwidths.

PRESENTATION OF MEASURED DATA

Noise Data for Launch- and Exit-Phase Flight

Internal measurements.- Plots of the overall internal sound-pressure levels as a function of time were obtained from playbacks of the recovered tape records of vehicles A and B and are shown in figure 7. In addition, the main events of each flight such as the lift-off, firing of the escape rocket system, and pylon separation are also indicated at the appropriate times on each record. For vehicle A it may be seen that the first peak in the sound-pressure-level time history occurs at lift-off and is due to the firing of the launch-vehicle engines. As the vehicle leaves the ground and accelerates, the sound-pressure levels reduce as a function of time to the instrument noise levels (approximate hash level). The sound-pressure level then subsequently builds up and reaches a maximum at about the time of maximum dynamic pressure as indicated in figure 2. The next significant event is noted to be the firing of the escape-system rocket engines. At times greater than 40 seconds the signal-to-noise ratio was not sufficient to obtain useful data.

For vehicle B very similar results were obtained with the following exceptions. Second-stage engines were added with the result that the elapsed time of the flight during which data were obtained is nearly twice as long as that for vehicle A. It can also be seen that the noise level of the instrumentation was lower in this latter case and thus data were obtained over a greater range of overall noise levels. As a matter of interest, frequency spectra have been determined at various times during the flight of each vehicle, and these data are presented in figures 8, 9, and 10.

The internal noise spectra in one-third octave bands due to the operation of the rocket engines at lift-off are presented in figure 8 for vehicles A and B. The most obvious result is that the spectra are very similar in shape. They are seen to contain two peaks, one occurring in the 100 cps band, and the second in the frequency range from

about 400 cps to 640 cps. The latter peak is in the range of frequencies corresponding to the frequencies of several of the natural vibration modes of the spacecraft. It should be noted that the engines of vehicle A had a different grain composition and about 10-percent less thrust than those of vehicle B. The difference in the noise levels may be due to possible burning instabilities.

One-third octave bandwidth frequency spectra for conditions where the noise of aerodynamic origin is believed to be the dominant component are shown in figures 9(a) and 9(b) for vehicles A and B, respectively. In each figure are noted the times measured from the time of lift-off, as indicated in figure 7, and the corresponding Mach numbers and dynamic pressures, as presented in figures 2 and 3, respectively. It may be seen that spectra obtained at various times during the flight of vehicle A have roughly the same shape and contain a single broad peak in the vicinity of 600 cps to 700 cps. In this respect these spectra, which are believed to be due to noise of aerodynamic origin, have shapes very similar to the spectra obtained at lift-off which is due to the operation of the launch-vehicle engines (fig. 8). The most obvious differences among the curves of figure 9(a) are in the one-third octave band levels, and these are noted to be higher for higher dynamic-pressure values. With regard to the data of figure 9(b), it can be seen that the same general conclusions apply. It is evident from comparing the data of vehicle B that the sound-pressure levels in the lower frequency bands are reduced and those in the higher frequency bands are increased. This results in a slight shift in the peak of the spectrum to a higher frequency at the higher Mach number and, in this respect, is similar to results obtained for a similar vehicle in reference 4. There are marked differences in the sound-pressure levels of vehicles A and B for comparable flight conditions, and these are illustrated in figure 10. One-third octave band spectra are presented for times during the flight of each vehicle when the free-stream dynamic pressure was about 2,000 lb/sq ft. The solid curve represents vehicle A for a Mach number of 2.0, whereas the two dashed curves represent vehicle B for Mach numbers of 1.6 and 3.8, respectively. Of particular significance is the fact that for approximately the same free-stream dynamic pressures, the measurements of vehicle A are markedly higher than those of vehicle B. This increase in one-third octave band level is believed to result from aerodynamic disturbances caused by the addition of a spoiler to the spacecraft of vehicle A (as noted in fig. 6) to increase the aerodynamic stability of the spacecraft.

Although the results of these tests and those of references 2 and 3 have indicated that the noise pressures increase generally as the dynamic pressure increases, it was noted that the maximum noise pressures did not always occur at the same time during the flight as the maximum dynamic pressure occurred. This phenomenon is illustrated in

figure 11 in which the local estimated dynamic pressure and the inside noise-pressure time histories are plotted for vehicle B. It can be seen that the peak in the noise-pressure curve is somewhat flattened and occurs at an earlier time than the peak in the dynamic-pressure curve. Furthermore, for the same dynamic pressures higher noise pressures are generally measured before the peak (at lower Mach numbers) than are measured after the peak (at higher Mach numbers). For example, when q has the value of 1,500 lb/sq ft at 24 seconds and 50 seconds, the value of $\sqrt{\bar{p}^2}$ is approximately 1.8 and 1.3, respectively. The preceding results may be due to the fact that the external noise spectrum shifts to higher frequencies at the higher speeds and that the transmission losses of the structure tend to be greater at these higher frequencies.

This Mach number effect is further illustrated along with the significance of external contouring by the internal noise data presented in figure 12. A dimensionless ratio of noise pressure to estimated local dynamic pressure is plotted as a function of Mach number for three different vehicles. The upper two curves are for vehicles A and B, respectively, and the curve for reference 4 applies to a vehicle similar in construction to vehicles A and B. It is believed that the noise-transmission characteristics for the data of the three curves in figure 12 are similar and thus the differences in the noise pressures are probably due mainly to the differences in the external contouring of the vehicles. An observation that can be made from the data of the figure is that at high Mach numbers there is a trend towards decreased inside noise pressures. This result is believed to be due to Mach number effects which have been described previously.

External measurements.- External surface-pressure measurements were obtained only for vehicle A by means of the probe microphone system described previously and illustrated schematically in figure 6. The external surface-pressure time history for vehicle A is presented in figure 13(a). Also included for comparison in figure 13(b) is the internal noise-level time history which has been replotted from figure 7(a). The main events of the flight such as lift-off, maximum dynamic pressure, and firing of the escape-system rockets are indicated in the figure. The first peak of the external time history trace occurs as a result of the firing of the rocket engine. The subsequent broad peak is believed to be due to noise of aerodynamic origin, and this is followed by a noise peak due to the firing of the escape-system rocket engines.

It may be noted that the shapes of the external and internal time history curves are markedly different. In particular, it can be seen that the broad peak due to noise of aerodynamic origin occurs at an earlier time in the external time history trace than it does in the internal time history trace. It is believed that the pressures measured at a point on the surface as in figure 13(a) are closely related

to the local flow conditions at that point and thus probably vary as a function of time, inasmuch as the Mach number, the dynamic pressure, and the altitude are varying. The time history trace of the internal noise level, on the other hand, represents a summation of the noise due to aerodynamic origin over a sizable area of the spacecraft surface, and within this area there may be rather large variations in the local flow conditions.

A distinguishing characteristic of the external surface-pressure data is the presence of relatively intense low-frequency components for the low Mach number range of the flight; this phenomenon is illustrated in figure 14 by the one-third octave band spectra which were obtained at various times during the flight and for which the corresponding Mach numbers and dynamic pressures differed. It may be seen from the figure that the spectra at Mach numbers of 0.55 and 1.10 are very similar in shape and are noted to contain very intense low-frequency components. The spectra for the higher Mach numbers are seen to be markedly different in shape, having less intense low-frequency components and more intense high-frequency components than the spectra obtained for the lower Mach numbers. Although the local flow conditions were not measured during these flights, regions of intense buffeting along the spacecraft surface have been indicated in unpublished data obtained at the Langley 2-foot transonic aeroelasticity tunnel.

L
1
1
3
4

The external data measured for vehicle A are shown in figure 15 where the ratio of external surface pressure to dynamic pressure is presented as a function of Mach number. Also shown in the figure is a dashed line representing the maximum-pressure-ratio values that would have been estimated on the basis of available wind-tunnel and low-speed flight data (refs. 6 and 7). The surface-pressure data measured for vehicle A are noted to be higher at most Mach numbers than the maximum-pressure-ratio values that would have been predicted for a vehicle with smooth aerodynamic surfaces. A distinguishing characteristic of the external surface pressures in the region of the highest measured values of figure 15 is the existence of large-amplitude low-frequency disturbances as indicated in the low Mach number spectra of figure 14. The presence of these intense low-frequency disturbances is believed in this case to result mainly from the presence of the aerodynamic spoiler shown schematically in the sketch of figure 6.

Noise Data During Firing of the Escape Rocket System

The escape rocket system functioned during the flight tests of vehicles A, B, and C. For vehicle A, the escape system was operated at a dynamic pressure estimated to be the maximum that would be encountered during operation of the Project Mercury spacecraft. For

vehicle B, the escape system was operated at altitude conditions corresponding to the maximum longitudinal acceleration obtained by the launch vehicle. For vehicle C, the escape system was operated at sea-level conditions and would correspond roughly to the conditions during launch. Noise measurements were made for all these operating conditions and, for vehicles A and B, are identified by corresponding peaks which are visible in the noise time history records. Although no time history record is presented for vehicle C, the one-third octave band frequency spectrum obtained at a point within the spacecraft during the escape rocket firing at about sea-level conditions is presented in figure 16. The spectrum is noted to have a rather broad peak, and in this respect is similar to the noise of aerodynamic origin spectra measured for the launch-vehicle rocket engines of vehicles A and B. There are, however, relatively higher noise levels at the higher frequencies. Although spectra were obtained during the firing of the escape-system rockets for vehicles A and B, it is believed that the corresponding spectra contain rather strong noise components of aerodynamic origin.

L
1
1
3
4

CONCLUDING REMARKS

Inside noise measurements have been made for three vehicles of the Project Mercury program and external noise measurements have been made for one vehicle of the Mercury program. The main sources of noise are noted to be the rocket engines during the launch phase and the noise of aerodynamic origin during the exit phase of the flight. The rocket noise was a maximum at lift-off and decreased rapidly as the vehicle gained altitude and speed. The aerodynamic noise increased generally as the dynamic pressure increased and was also affected significantly by the Mach number and the external contouring of the vehicle.

Because of the difficulty of obtaining data for noise of aerodynamic origin, the flight information presented herein is valuable and unique. However, there is obvious need for further work in resolving various effects of Mach number and dynamic pressure for supersonic and hypersonic speeds.

Langley Research Center,
National Aeronautics and Space Administration,
Langley Air Force Base, Va., October 13, 1961.

REFERENCES

1. Von Gierke, H. E.: Vibration and Noise Problems Expected in Manned Space Craft. Noise Control, vol. 5, no. 3, May 1959, pp. 9-16.

2. Nadel, Aaron B.: Auditory Noise and Vibration Problems for Manned Space Vehicles. Res. Memo. RM 59TMP-50, Gen. Elec. Co., Oct. 20, 1959.

3. Franken, Peter A., Kerwin, Edward M., Jr., and the Staff of Bolt Beranek and Newman, Inc. (Cambridge, Mass.): Methods of Flight Vehicle Noise Prediction. WADC Tech. Rep. 58-343, ASTIA Doc. No. AD 205776, U.S. Air Force, Nov. 1958.

4. Hilton, David A., Mayes, William H., and Hubbard, Harvey H.: Noise Considerations for Manned Reentry Vehicles. NASA TN D-450, 1960.

5. Anon.: Standard Atmosphere - Tables and Data for Altitudes to 65,800 Feet. NACA Rep. 1235, 1955. (Supersedes NACA TN 3182.)

6. Eldred, Ken: Prediction of Sonic Exposure Histories. Proceedings of the Symposium on Fatigue of Aircraft Structures. WADC Tech. Rep. 59-507, U.S. Air Force, Aug. 1959, pp. 396-415.

7. Willmarth, William W.: Wall Pressure Fluctuations in a Turbulent Boundary Layer. NACA TN 4139, 1958.

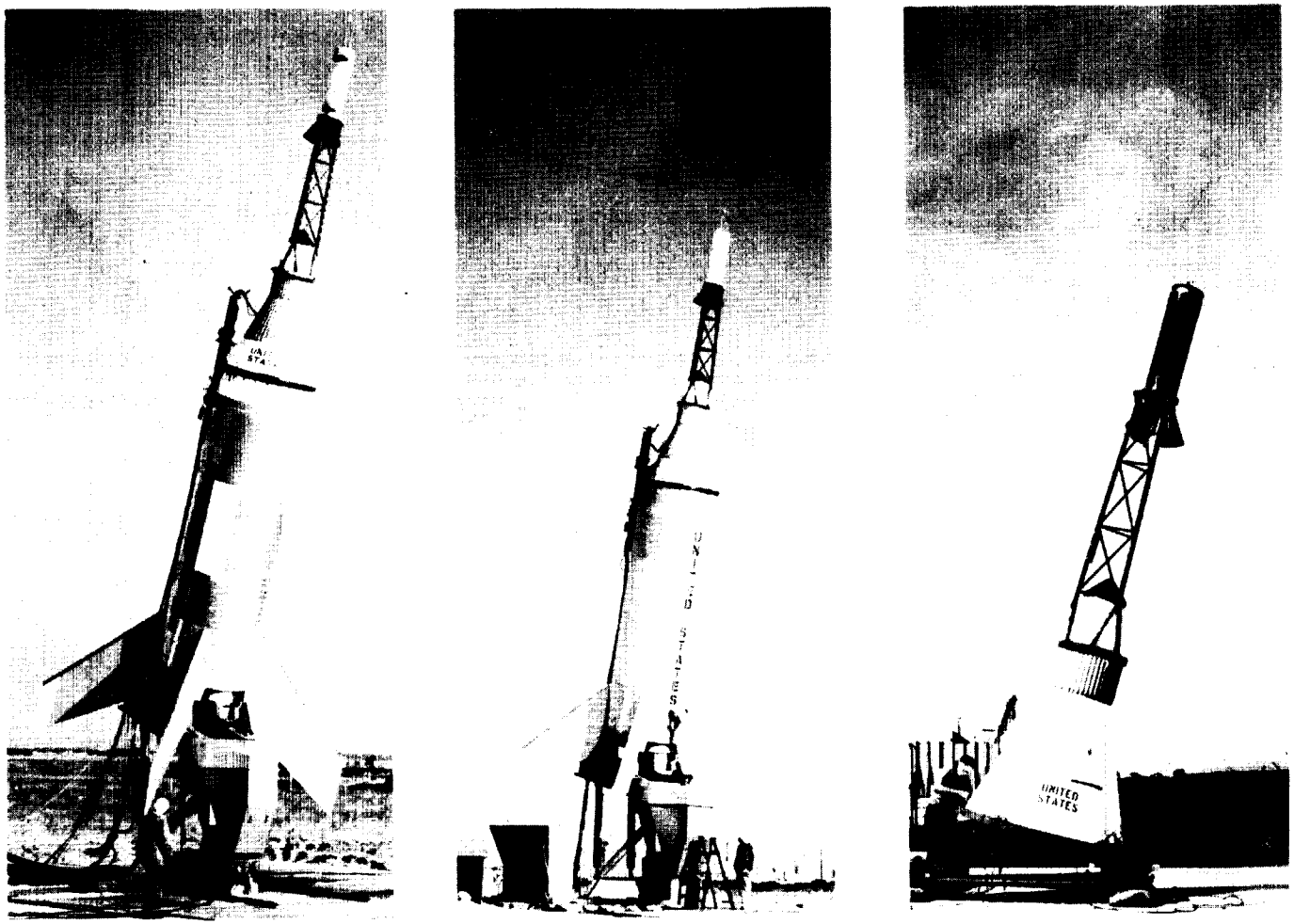

L-61-5119

(a) Vehicle A (Little Joe 1B with spacecraft).

(b) Vehicle B (Little Joe 2 with spacecraft).

(c) Vehicle C (spacecraft).

Figure 1.- Photographs of test vehicles and launchers.

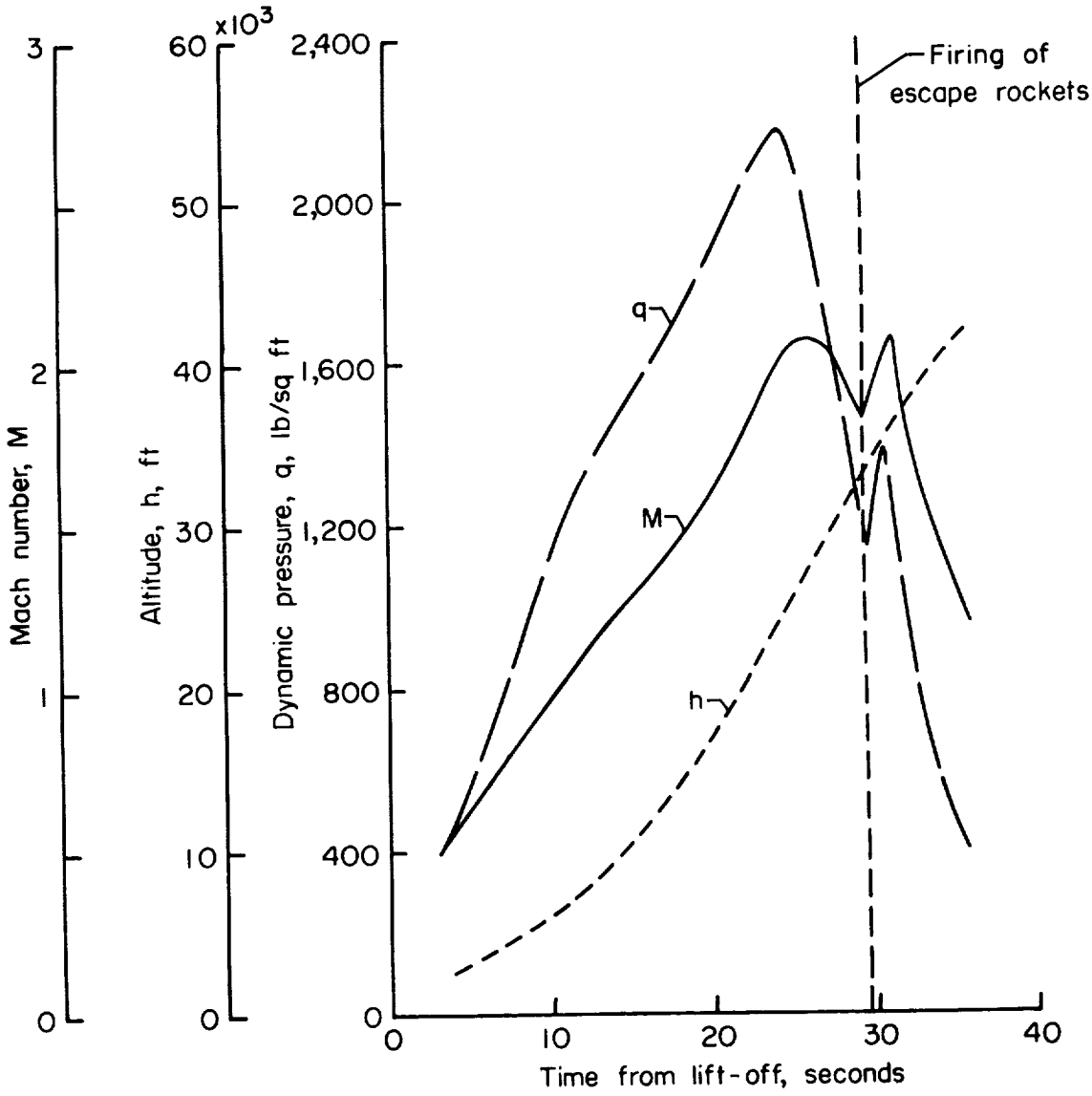

Figure 2.- Time history of Mach number, altitude, and dynamic pressure for vehicle A for which noise data were obtained.

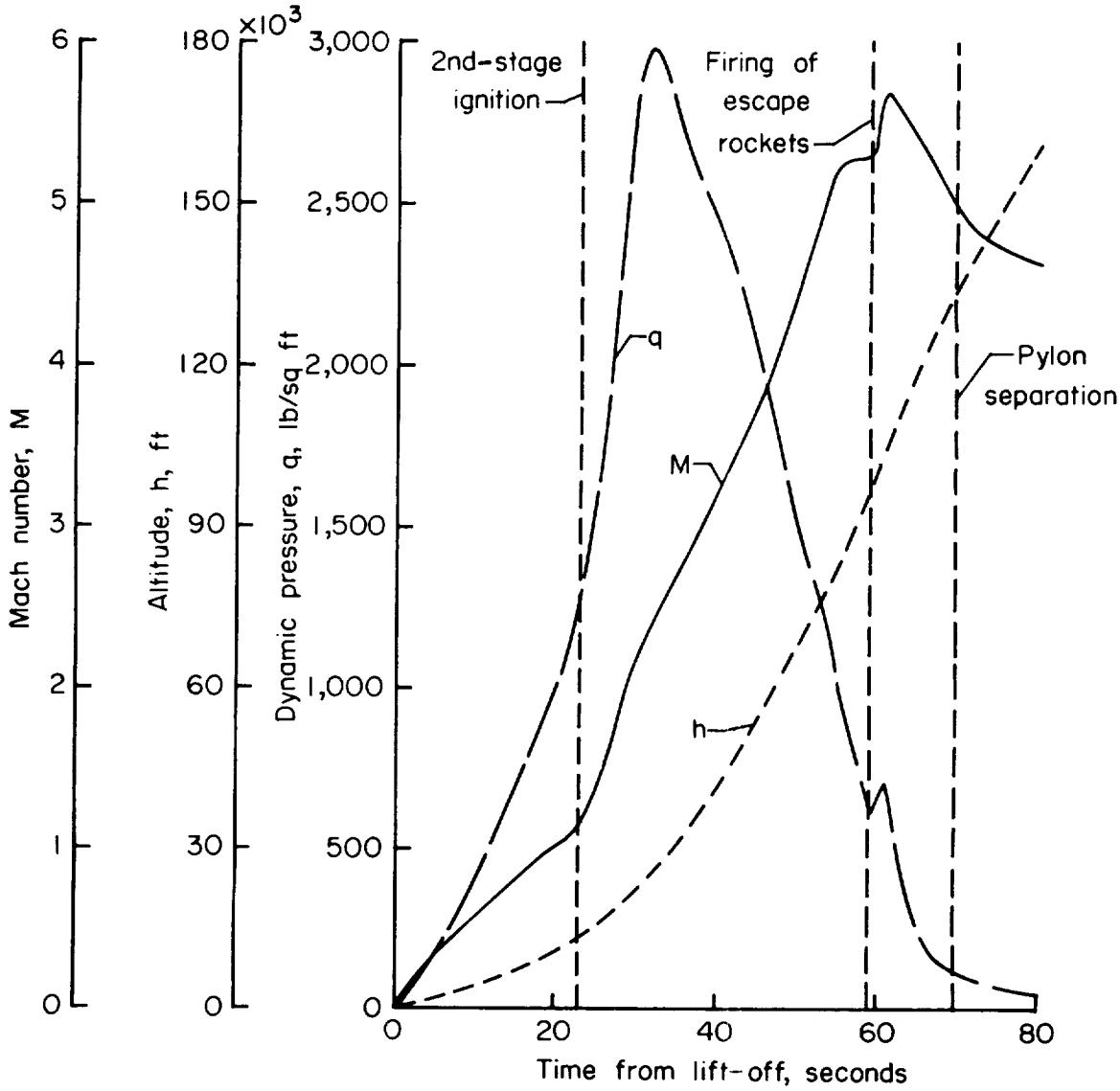

Figure 3.- Time history of Mach number, altitude, and dynamic pressure for vehicle B for which noise data were obtained.

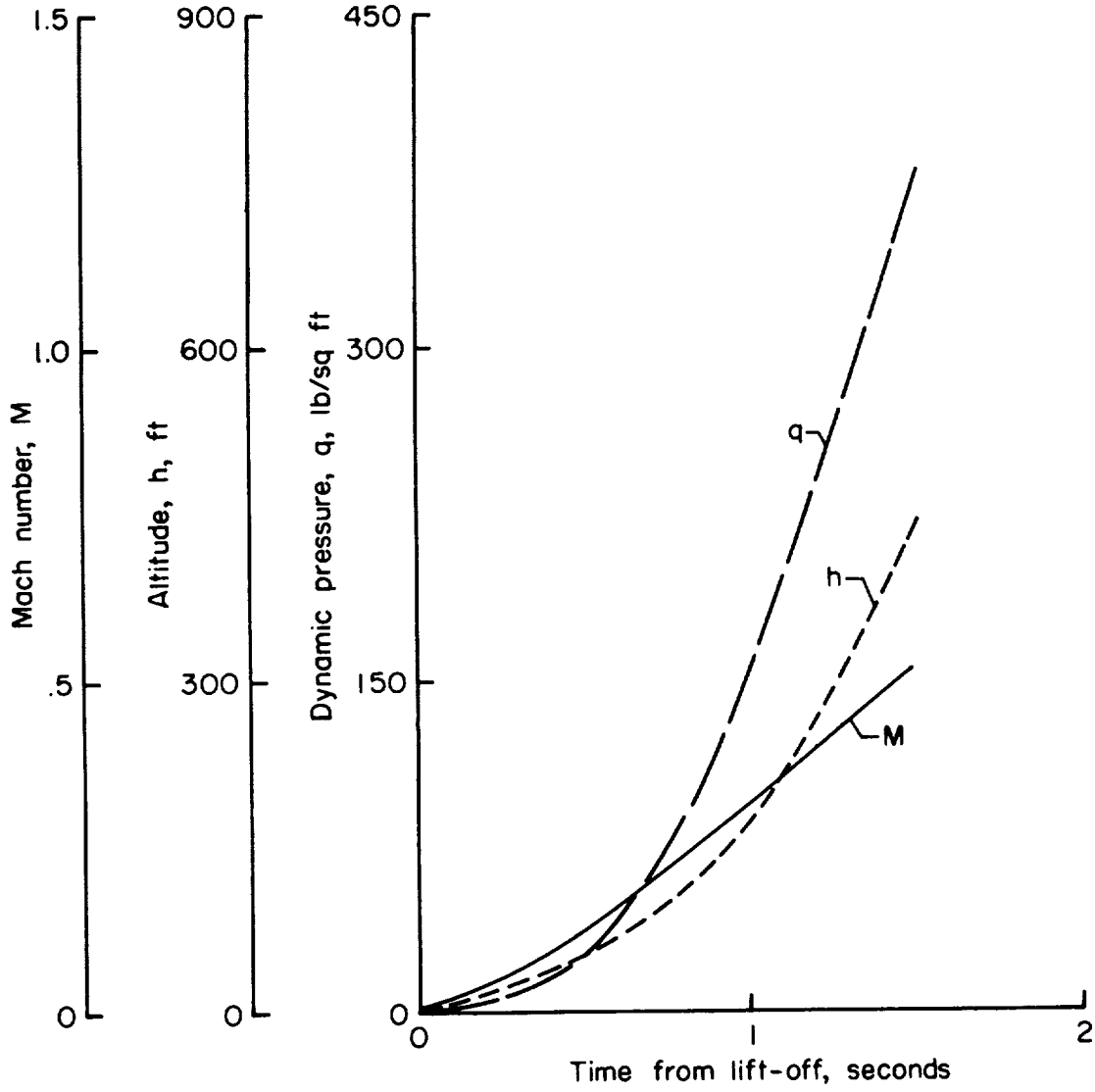

Figure 4.- Time history of Mach number, altitude, and dynamic pressure for vehicle C for which noise data were obtained.

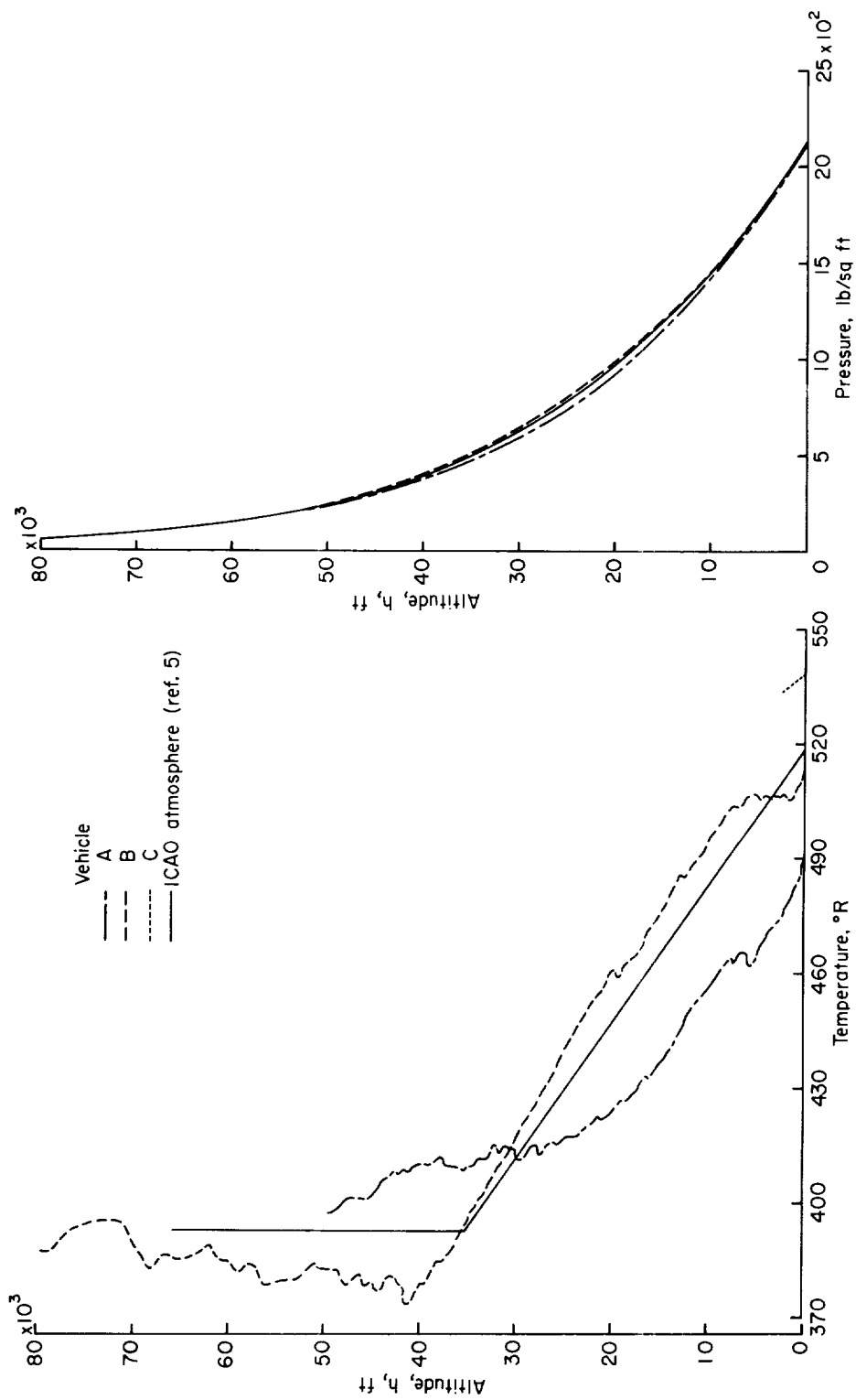

Figure 5.- Data obtained from atmospheric soundings.

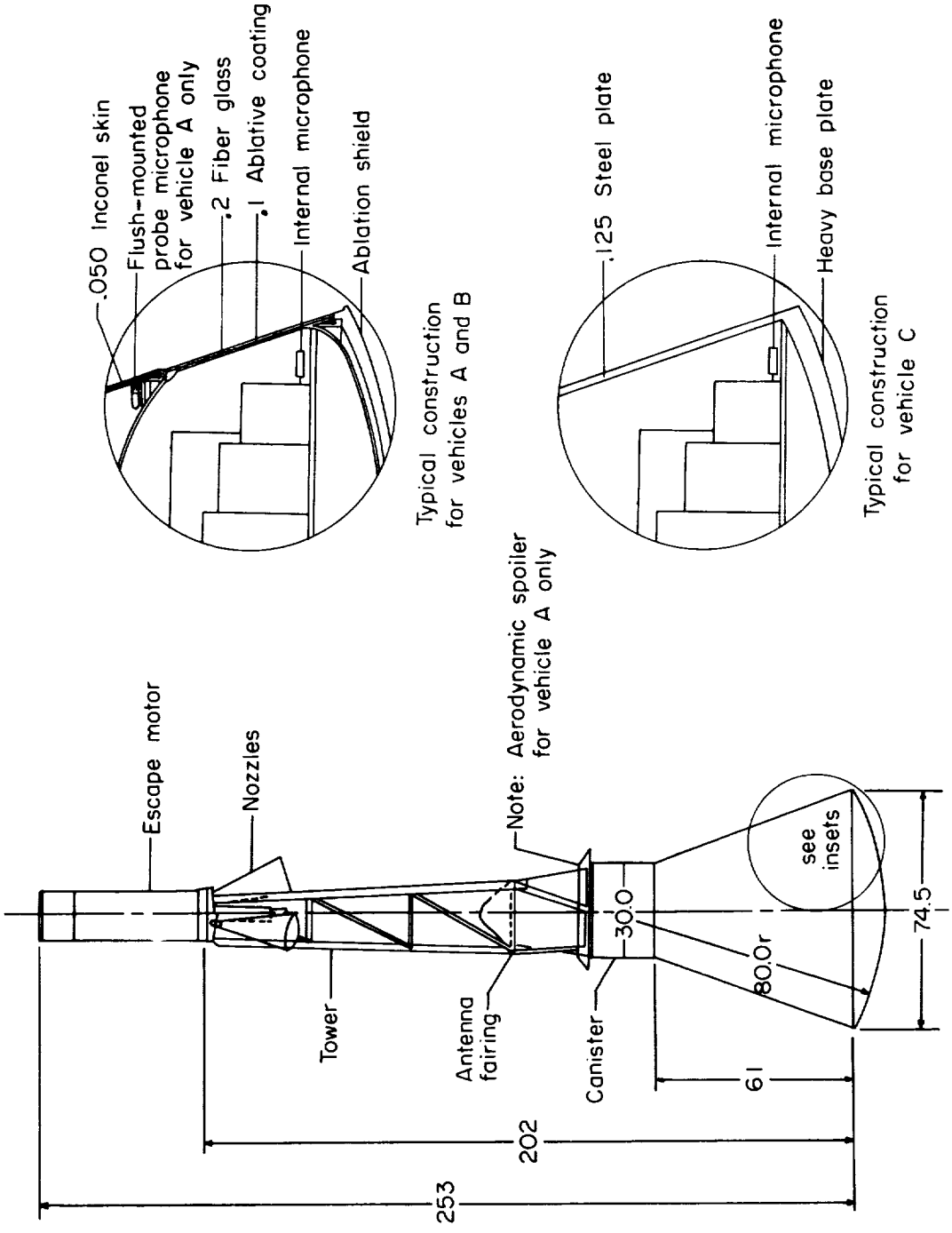

Figure 6.- Sketch of spacecraft. All dimensions are in inches.

L-11344

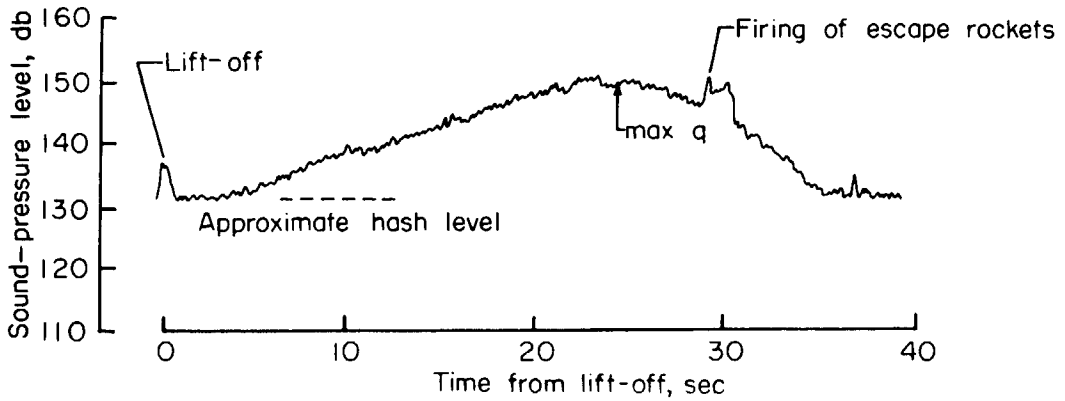

(a) Vehicle A.

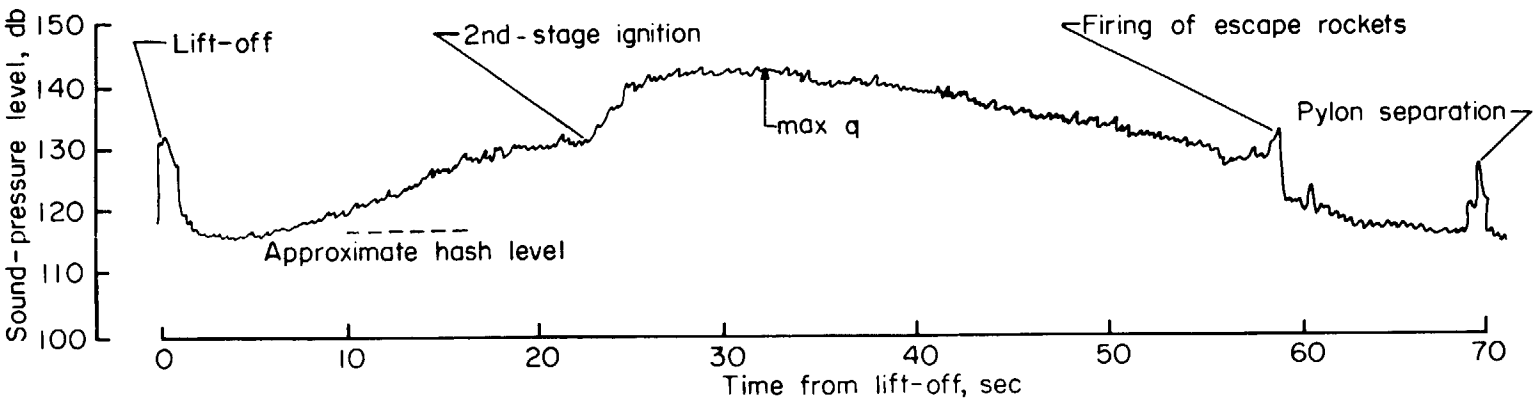

(b) Vehicle B.

Figure 7.- Time history of overall internal sound-pressure levels.

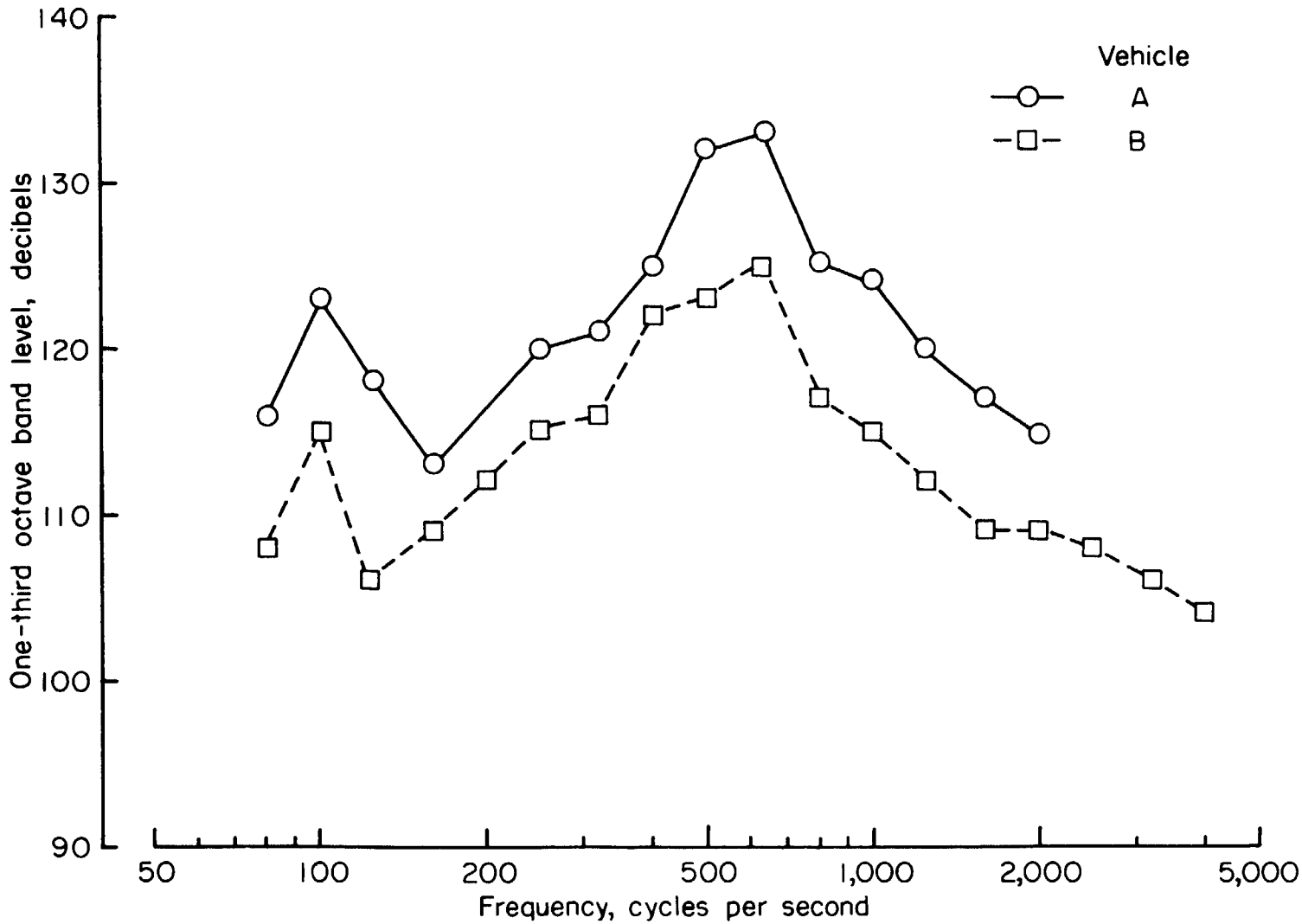

Figure 8.- Noise spectra inside spacecraft of vehicles A and B at lift-off.

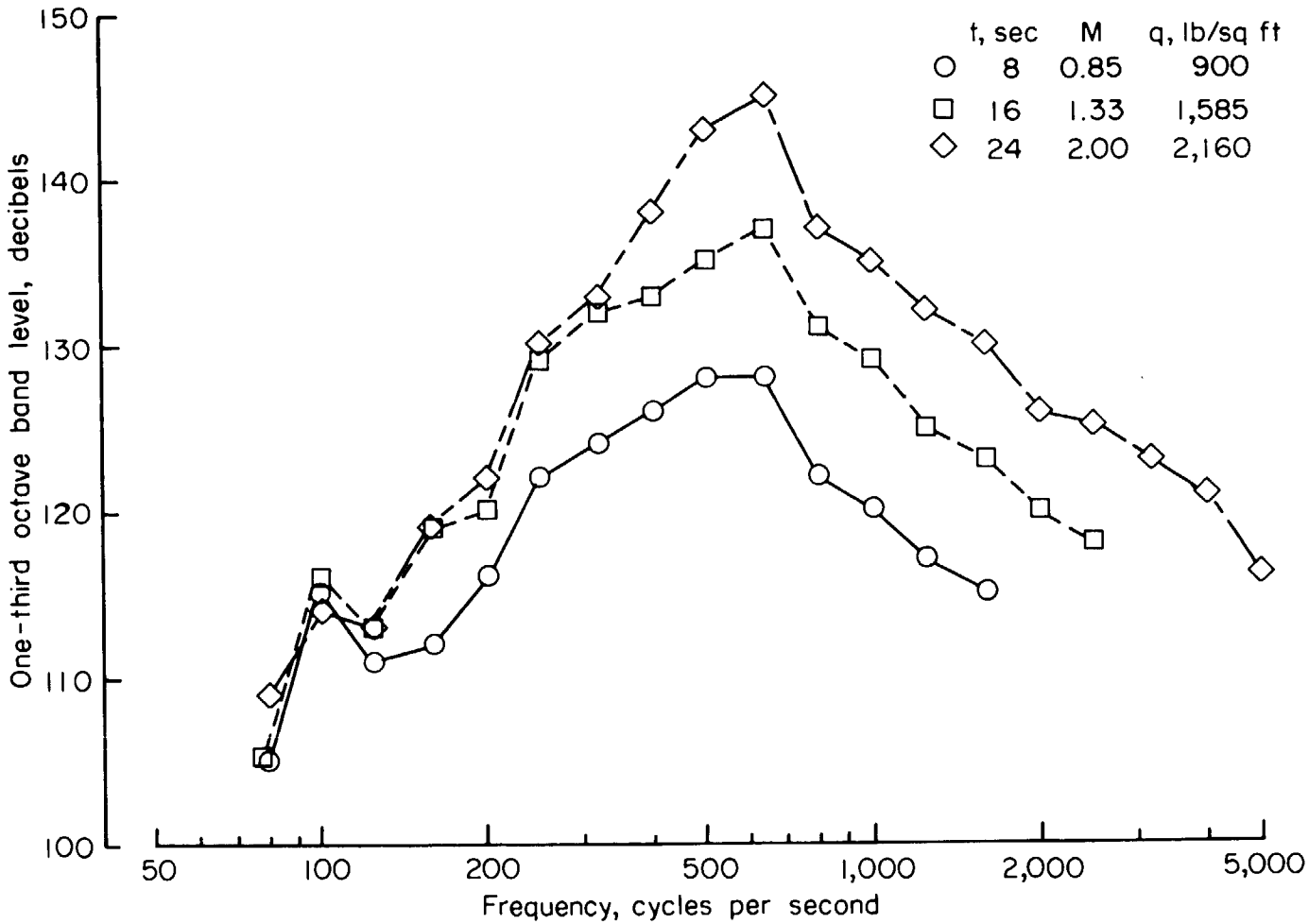

(a) Vehicle A.

Figure 9.- Noise spectra of aerodynamic origin inside spacecraft of vehicles A and B at various flight times.

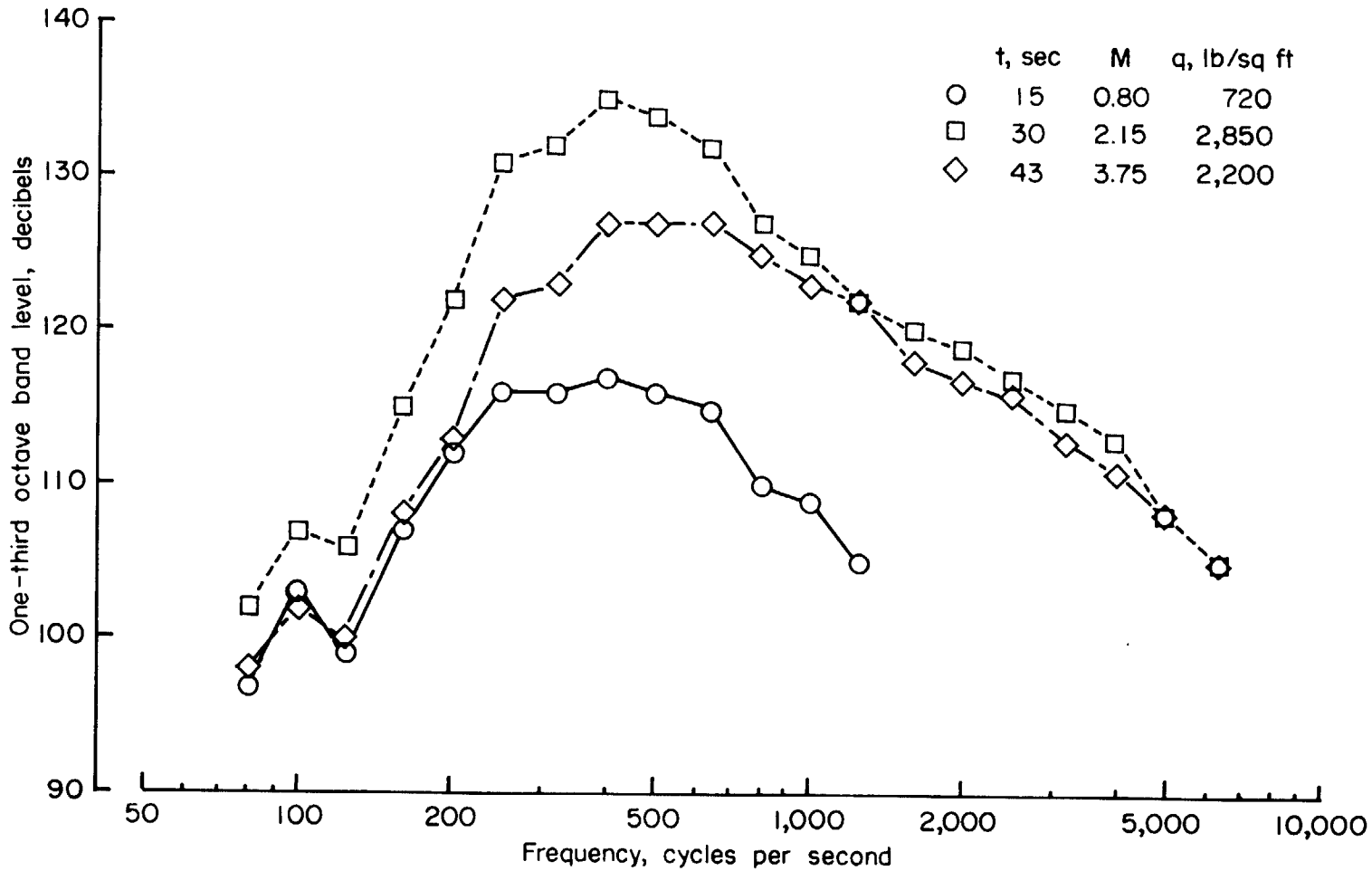

(b) Vehicle B.

Figure 9.- Concluded.

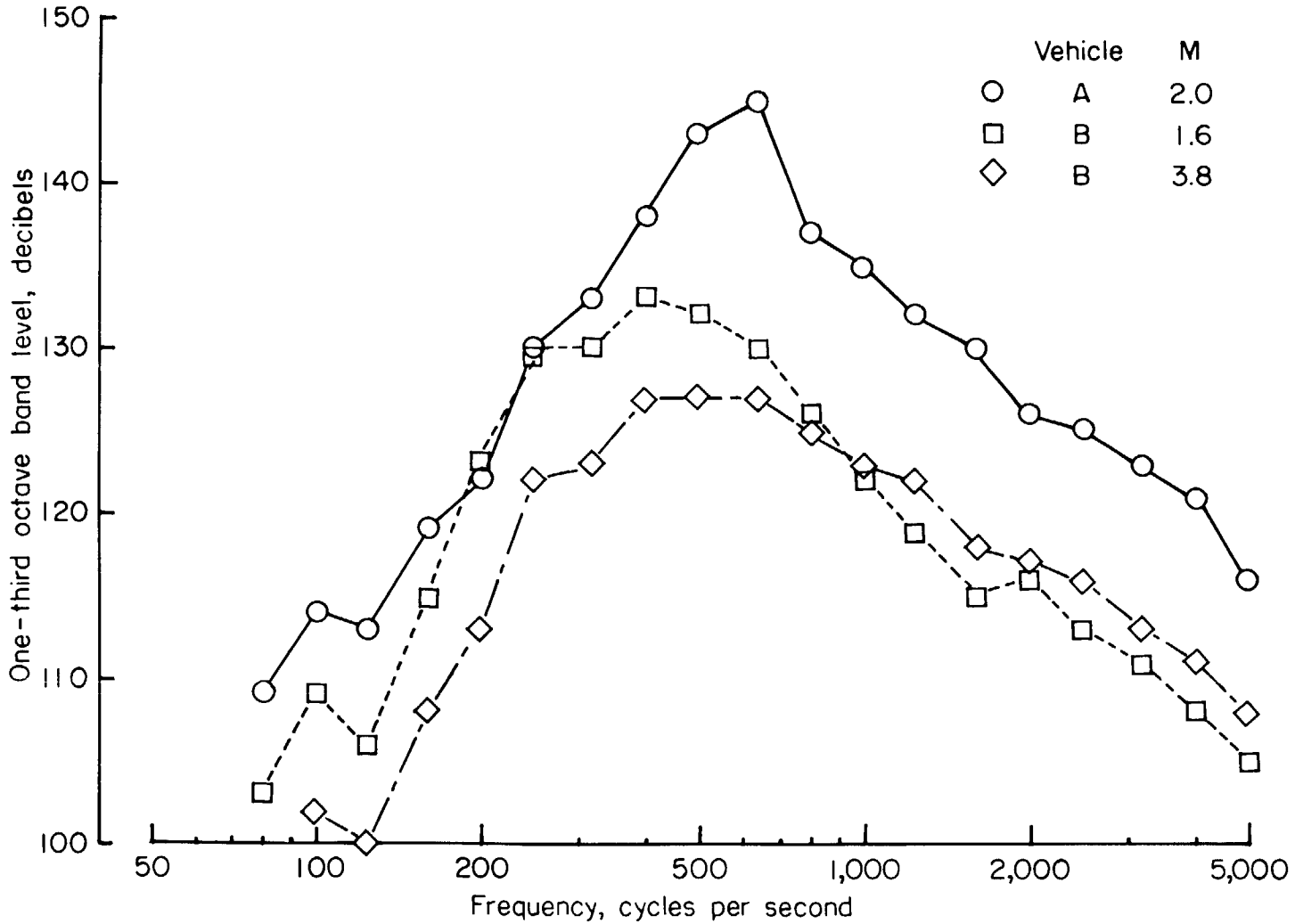

Figure 10.- Noise spectra of aerodynamic origin inside spacecraft of vehicles A and B for conditions of approximately equal free-stream dynamic pressures of 2,000 lb/sq ft.

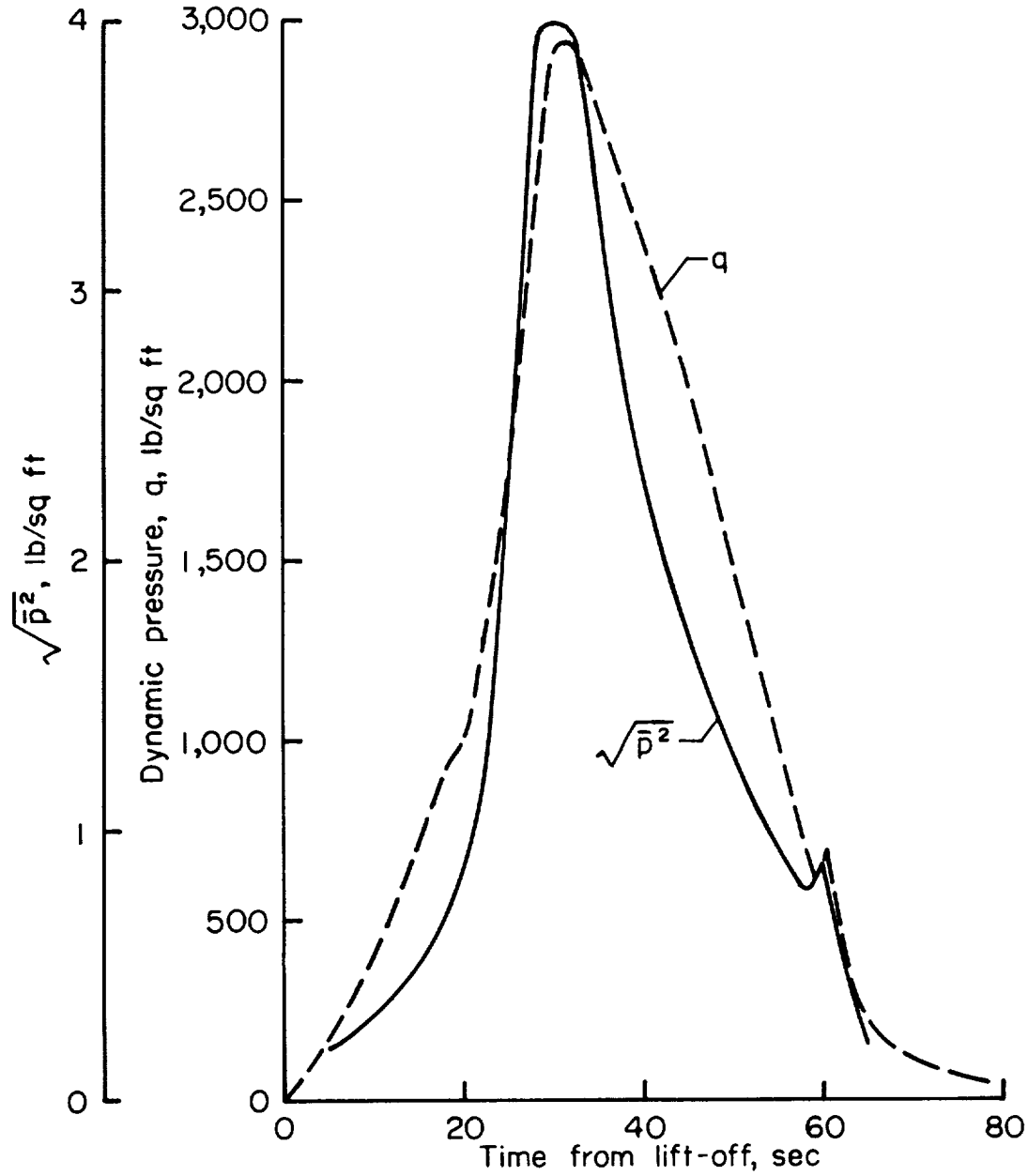

Figure 11.- Time histories of free-stream dynamic pressures and inside noise pressures for vehicle B.

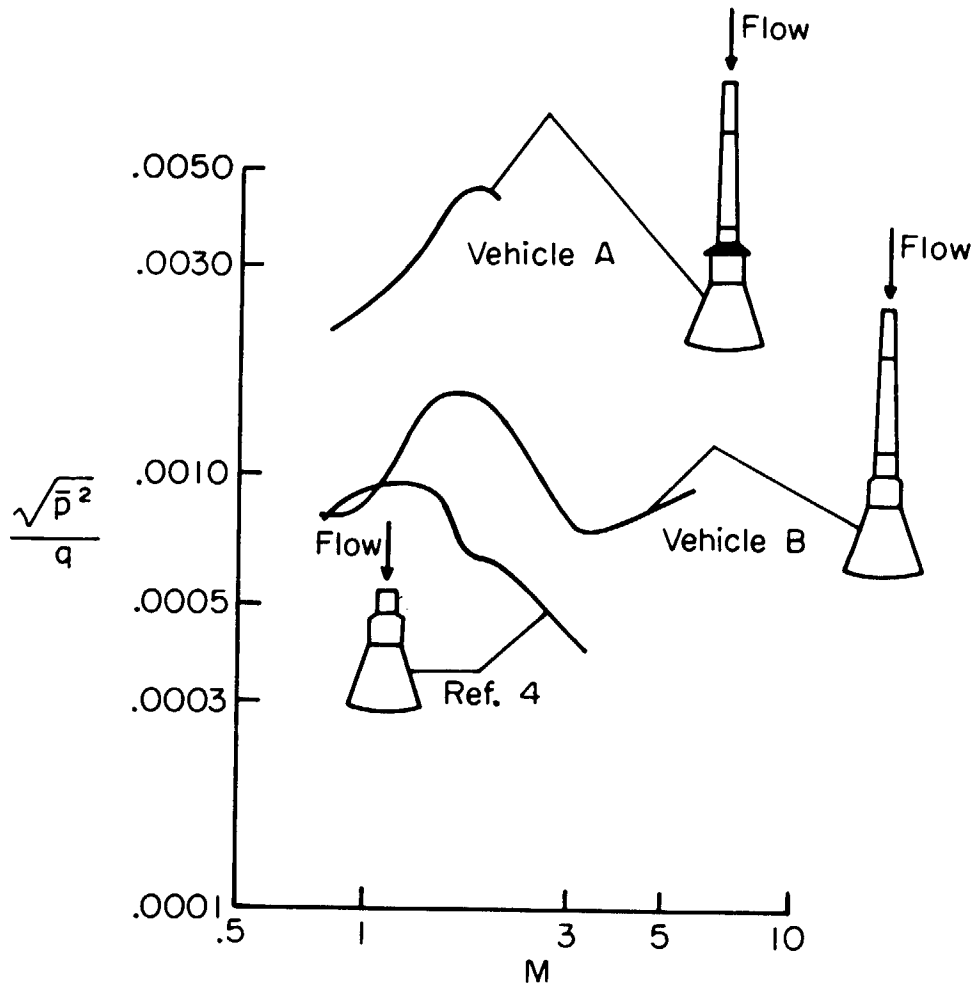

Figure 12.- Ratios of internal noise pressure to estimated local dynamic pressure as a function of free-stream Mach number.

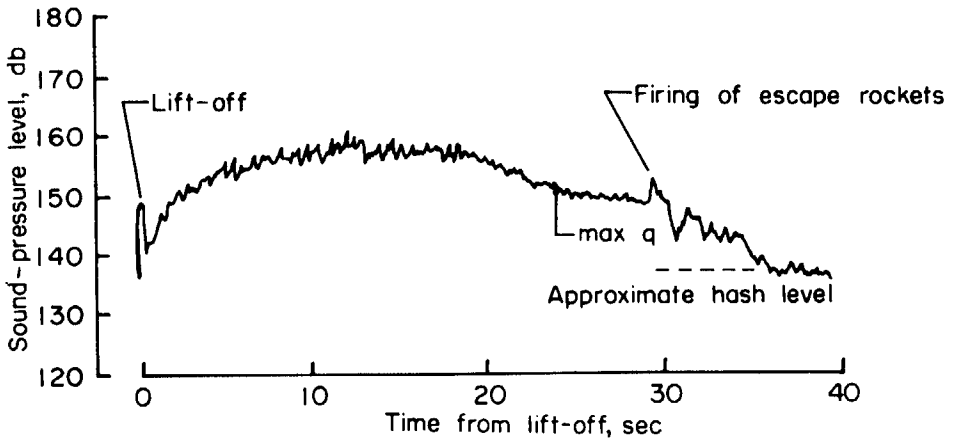

(a) External surface-pressure levels.

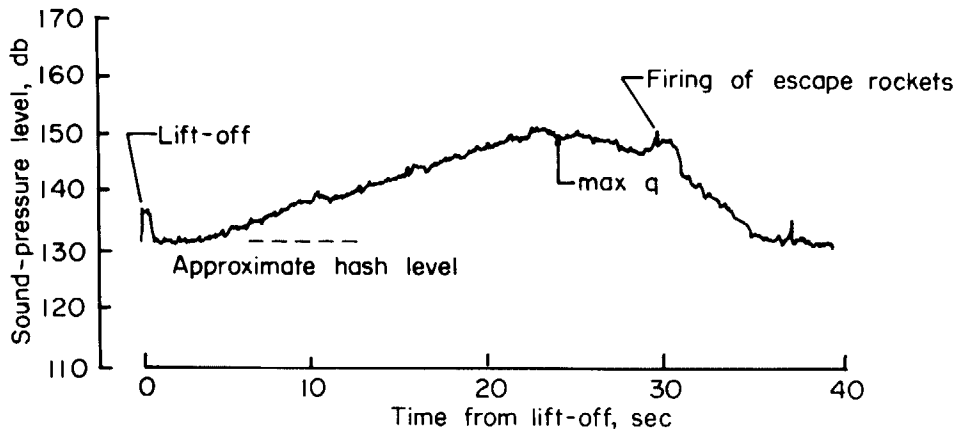

(b) Internal noise levels.

Figure 13.- External surface pressures and internal noise-pressure-level time histories for vehicle A.

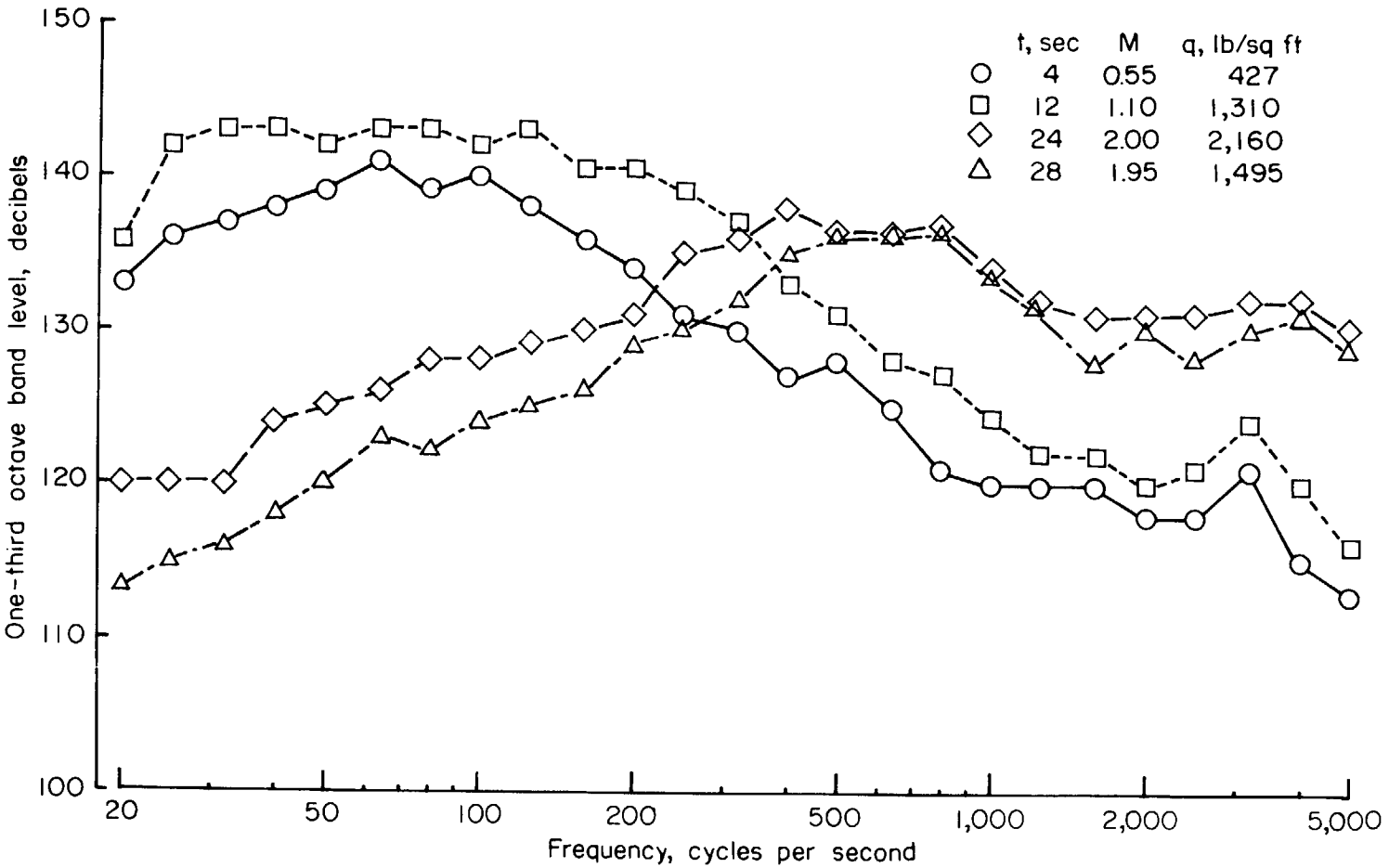

Figure 14.- External surface-pressure spectra for vehicle A at several Mach numbers.

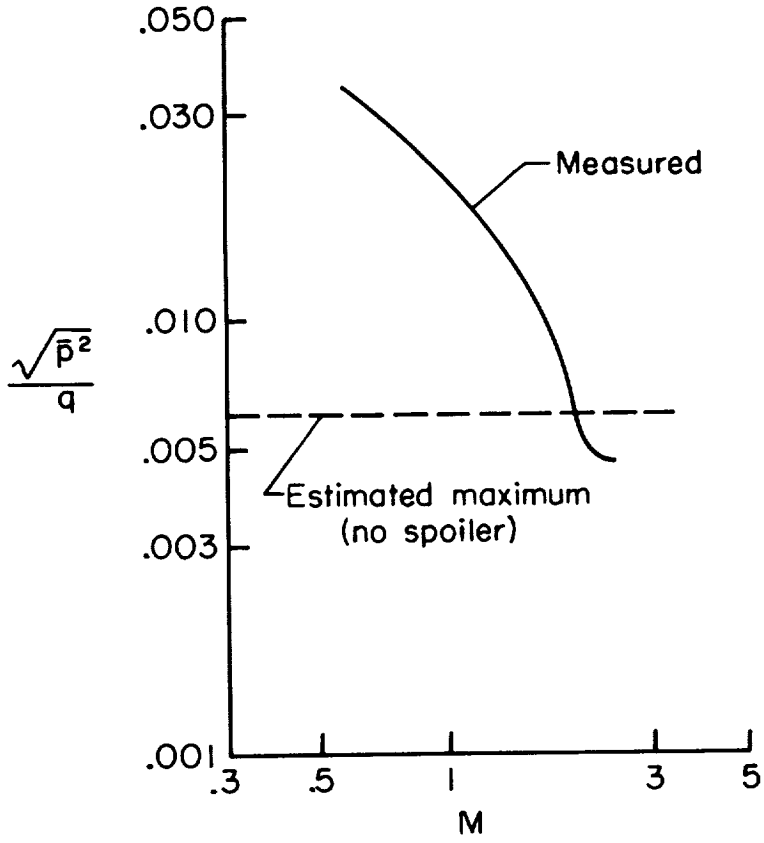

Figure 15.- Ratios of external surface pressure to estimated local dynamic pressure as a function of free-stream Mach number for vehicle A.

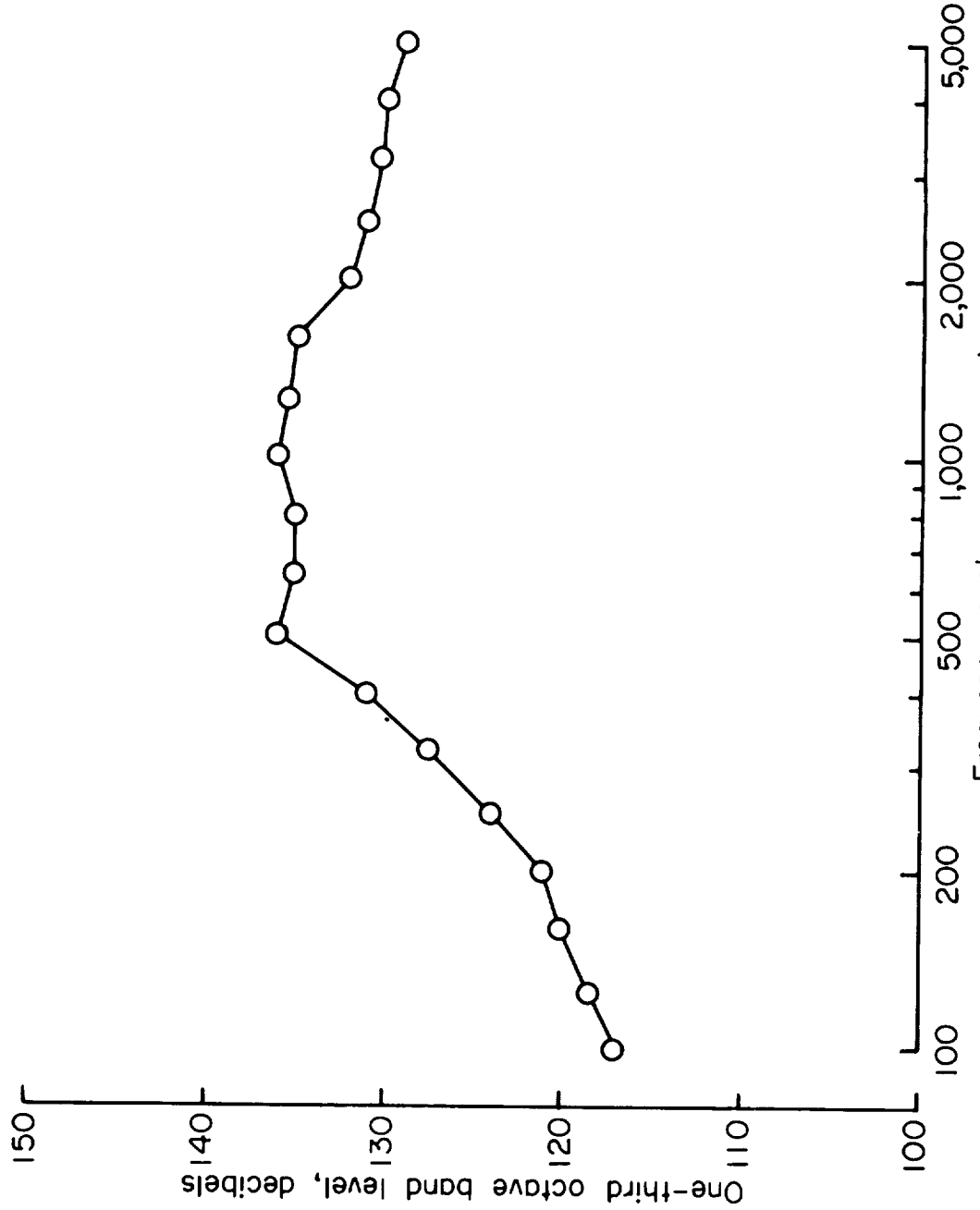

Figure 16.- Noise spectrum measured inside vehicle C during firing of the escape rocket engines at about sea-level conditions. (Adjusted from spectrum obtained with a 100-cps constant bandwidth analyzer.)

L-1134

NASA-Langley, 1962 L-1134